Small 13.33 (2017): 1700965

DOI: https://doi.org/10.1002/smll.201700965

Multi-stimuli response micro- and nano-layers of a coordination polymer based on Cu_2I_2 chains linked by 2-aminopyrazine

J. Conesa-Egea,
Departamento de Química Inorgánica, Universidad Autónoma de Madrid, 28049 Madrid, Spain

J. Gallardo-Martínez,
Departamento de Química Inorgánica, Universidad Autónoma de Madrid, 28049 Madrid, Spain

Prof. S. Delgado,
Departamento de Química Inorgánica, Universidad Autónoma de Madrid, 28049 Madrid, Spain; Institute for Advanced Research in Chemical Sciences (IAdChem), Universidad Autónoma de Madrid, 28049 Madrid, Spain

Dr. J. I. Martínez,
Departamento de Nanoestructuras, Superficies, Recubrimientos y Astrofísica Molecular, Instituto de Ciencia de Materiales de Madrid (ICMM-CSIC), 28049 Madrid, Spain

Dr. J. Gonzalez-Platas,
Servicio de Difracción de Rayos X (SIDIX). Departamento de Física, Universidad de La Laguna, Avda. Astrofísico Fco. Sánchez s/n, La Laguna, Tenerife, E-38204, Spain

Dr. V. Fernández-Moreira,
Departamento de Química Inorgánica, Instituto de Síntesis Química y Catálisis Homogénea (ISQCH), CSIC-Universidad de Zaragoza, 50009 Zaragoza, Spain

Dr. U. R. Rodríguez-Mendoza,
Instituto de Materiales y Nanotecnología (IMN). Departamento de Física, Universidad de La Laguna, Avda. Astrofísico Fco. Sánchez s/n, La Laguna, Tenerife, E-38204, Spain

Prof. P. Ocón,
Departamento de Química Física Aplicada, Universidad Autónoma de Madrid, 28049 Madrid, Spain

Dr. F. Zamora, and
Departamento de Química Inorgánica, Universidad Autónoma de Madrid, 28049 Madrid, Spain; Institute for Advanced Research in Chemical Sciences (IAdChem), Universidad Autónoma de Madrid, 28049 Madrid, Spain; Condensed Matter Physics Center (IFIMAC), Universidad Autónoma de Madrid, 28049 Madrid, Spain

Dr. P. Amo-Ochoa*
Departamento de Química Inorgánica, Universidad Autónoma de Madrid, 28049 Madrid, Spain; Institute for Advanced Research in Chemical Sciences (IAdChem), Universidad Autónoma de Madrid, 28049 Madrid, Spain

---

pilar.amo@uam.es.
Dedicated to Prof. Julio Gómez Herrero

Abstract

A non-porous laminar coordination polymer of formula $[Cu_2I_2(2\text{-aminopyrazine})]_n$ has been prepared by direct reaction between CuI and 2-aminopyrazine, two industrially available building blocks. The fine tuning of the reaction conditions allows obtaining $[Cu_2I_2(2\text{-aminopyrazine})]_n$ in micrometric and nanometric sizes with same structure and composition. Interestingly, both materials show similar reversible thermo- and pressure-luminescent response as well as reversible electrical response to volatile organic solvents such as acetic acid. X-ray diffraction studies under different conditions, temperatures and pressures, in combination with theoretical calculations allow rationalizing the physical properties of this compound and its changes under physical stimuli. Thus, the emission dramatically increases when lowering the temperature, while an enhancement of the pressure produces a decrease in the emission intensity. These observations emerge as a direct consequence of the high structural flexibility of the Cu_2I_2 chains which undergo a contraction in Cu-Cu distances as far as temperature decreases or pressure increases. However, the strong structural changes observed under high pressure lead to an unexpected effect that produces a less effective Cu-Cu orbital overlapping that justifies the decrease in the intensity emission. This work shows the high potential of materials based on Cu_2I_2 chains for new applications.

Keywords

coordination polymers; stimuli response materials; nanomaterials; multifunctional materials

---

1 Introduction

Multifunctional materials, and more specifically those presenting stimuli-response, are of great interest due to their ability to bring and combine remarkable physical properties with a change in these properties when exposed to a physical and/or chemical stimulus. Among other properties they can combine luminescence,[1] non-linear optics, magnetism[2] and/or electrical conductivity[3] which enable the development of new devices and commercial applications, *i.e.*, thermochromics in paints,[4] plastics and textiles,[5] electrochromics in car mirrors, and smart windows.[6] Additionally, materials showing solvatochromism and mechanochromism are promising candidates for the development of memory devices, motion or damage sensors.[3, 7] Within this context, the development of multi-stimuli-responsive materials is quite meaningful for ever-growing multiple requirements, *e.g.*, simultaneous mechanochromic and thermochromic luminescence or temperature and pressure sensors. Some of these materials are required in case of low energy consumption and high information processing power multielectronic equipment useful in different industrial sectors such as space, aerospace, aeronautics as well as in nuclear fields or packaging and store industries.[8]

One subclass of multifunctional materials consists of those based on coordination polymers (CPs). CPs show a large variety of tunable architectures and chemical functionalities, achieved by the suitable selection and chemical combination of their fundamental building blocks, organic molecules acting as ligands and the metal ion entities.[9] CPs have shown interesting physico-chemical properties and are a current source of multifunctional

materials. Indeed, some few of them have been already commercialized as catalysts, as well as for specific gas store and/or separation.[10]

Additionally, CPs are also a potential source of novel nanomaterials. They have been prepared as nanoparticles, fibers and nano-layers.[9, 11] Moreover, the synthesis of nanostructures with response to physical and/or chemical stimuli is of high interest because of their potential implementation in the fabrication of electrical, mechanical or optical components of novel miniaturized devices.[12]

Within CPs those containing d^{10} are well-known for their high structural diversity and versatility, rich photophysical behavior, interesting electrical properties and high luminance efficiency.[13] In particular, the use of halogen or pseudo halogen as bridge ligands and pyridine or pyrazine derivatives as terminal or bridge ligands respectively, enable the formation of a variety of d^{10} metal CPs architectures from 1D to 3D, some of them showing interesting properties.[14] Moreover, it is already known that compounds showing metallophilic interactions can provide multi-stimuli chromophore materials able to respond to environmental stimuli with a marked change in their photophysical properties.[15] Indeed, CPs based on $[CuIL]_n$ chains are excellent candidates for the production of multiply stimuli-responsive materials.[16] In fact, we have recently proved that Cu-I double chains bearing substituted aminopyridine ligands are stimuli-responsive materials towards both chemical and physical stimuli.[13a, 17] This behavior is due to the high structural flexibility of the Cu-I double chain and the presence of terminal ligands bearing functional groups available for H-bond interaction with guest molecules. Consequently, the presence of organic ligands with molecular recognition capabilities enables the possibility to obtain a kind of novel molecular sensors.[18] In addition to their selective detection ability, e.g. small molecules, these materials could also play a significant role for the discovery of new environmental and biomedical applications.[19]

In this work, we present a novel non-porous laminar coordination polymer based on Cu^{I}-I chains connected *via* 2-aminopyrazine, with formula $[Cu_2I_2(Apyz)]_n$ (2-aminopyrazine=Apyz), which shows reversible thermo- and pressure-luminescent response as well as reversible electrical response to volatile organic solvents such as acetic acid. The adjustment of the synthetic conditions has allowed obtaining this material as nanosheets with nanometric thicknesses (**1n**) or as micrometric crystals (**1m**) both with the same structure and composition. The physical properties of **1n** and **1m** have been studied and compared. Nano-layers of $[Cu_2I_2(Apyz)]_n$ with thicknesses of few molecules have been isolated by liquid phase exfoliation of **1m**. Theoretical studies have been carried out in order to understand the physical properties of the material and its changes under several stimuli.

2 Results and Discussion

2.1 Preparation, Structural and Morphological Characterization of $[Cu_2I_2(Apyz)]_n$

The direct reaction between copper(I) iodide and 2-aminopyrazine (Apyz) under solvothermal conditions gives rise to the isolation of micron-sized crystals of a 2D coordination polymer with formula $[Cu_2I_2(Apyz)]_n$ (**1m**). The X-ray crystal structure of **1m** measured at atmospheric pressure and room temperature consists of a very simple

asymmetric unit (Figures 1 and S1). Each copper(I) atom is four-coordinated to three iodine atoms and the iminic nitrogen of the organic ligand (Figures 1b and S2, Tables S1 and S2).

The amino group in these ligands is delocalized with a 50 % probability between two positions in each 2D sheet (Figure 1b). The coordination network is established by a polymeric *staircase* motif of copper-iodine chains that are connected by the two iminic nitrogen atoms in each 2-aminopyrazine ligands leading to a two-dimensional structure (Figures 1a and S2).

Interestingly, the direct reaction between copper(I) iodide and 2-aminopyrazine (Apyz) carried out at room temperature under magnetic stirring led to the formation of a nanometric crystalline material **1n**, showing the same composition and structure (powder X-ray diffraction in Figure S3) to those found in **1m**.

The morphological analysis of **1m** and **1n**, carried out by SEM, shows significant differences in shape and size (Figure 2). Thus, **1m** consists of crystals with lateral dimensions (38±10) x (21±7) μm^2 (Figure S10a). The edge of the crystals is not even; it is formed of smaller sheets which suffer a coalescence process, causing the crystal growth (Figure S10b, c). With the aim to reduce the thickness of the material, water suspensions of the sonicated samples of **1n** were prepared and deposited *via* drop-casting on SiO_2 (Figure 2c-d). The mean lateral dimensions of **1n** are (372±127) × (1209±300) nm^2 while the estimated thickness is 51±21 nm^3 (Figure S11). AFM images show sheet aggregates with a height distribution ranging from 5 to 20 nm, up to 300 nm when piled up, and lateral dimensions *ca.* 500×2500 nm^2 (Figure 3 and Figure S12). In view of these results, ultrasound exfoliates the polymer giving rise to nanoflakes with *ca.* 10-32 stacked monolayers (this data is obtained when comparing the height profile obtained by AFM with the height of a single sheet obtained by diffraction of x-ray of single crystal, see Figures 1a and 3). Interestingly we notice that all the **1n** nanolayers are very flat.

2.2 Physical Properties

2.2.1 Thermochromic bevahior—Photophysical properties of CPs based on d^{10} metal centers are in current interest. Particularly those CPs containing Cu(I) as building block may show bright luminescence emission, varying from blue to red light. Therefore, they have attracted recent attention towards potential applications.[15, 20] Previous works have shown that the emission energies of Cu(I)-iodide complexes are strongly affected by the presence of heterocyclic organic ligands linked to the metal center of the $[Cu_nI_n]$ chains, mainly due to structural changes induce by the presence of these terminal ligands and/or their supramolecular interactions.[14d, 14e] Mostly, the luminescent emissions observed are assigned to iodide-to-copper(I) charge transfer (IMCT), metal to ligand charge transfer (MLCT), halogen-to-ligand charge transfer (ILCT), cluster-centered (CC) transition, or the admixture of more than one of these contributions. Therefore, we decided to evaluate the solid-state luminescence behavior of both micrometric size crystal (**1m**) and nanometer size powder (**1n**). Thus, excitation of solid crystalline samples **1m** and **1n** with an UV lamp (λ_{exc} = 365 nm), at room temperature, produces a very weak orange emission for both materials (Figure 4a, c). However, upon cooling at 80 K both **1m** and **1n** significantly increase their

emission intensity showing a perceptive eye shift from orange to yellow (Figure 4b, d). The thermochromic process is fully reversible for **1m** and **1n**.

In order to evaluate in more detail these seminal experimental observations, emission spectra at variable temperature of **1m** and **1n** were recorded (Figures 5 and S13), observing similar results for both (**1m** and **1n**) (for additional data see SI section S3). Thus, by lowering the temperature of **1m** from 300 to 80 K, a progressive increase of the emission intensity (30 times higher at 80 K than at 300 K) and a blue-shift were observed. The very weak emission observed at *ca.* 630 nm at 300 K, is progressively shifted to 566 nm at 80 K (Figure 5). The lifetime measured at 80 K was 20.9 μs, which falls in the microsecond-order decay lifetime and is assigned to phosphorescence, arising from a triplet state. Essentially, the size of the sample seems to influence mainly in the emission intensity, which is lower in the case of nanosized material **1n** (Figure S13).

Additionally, in order to evaluate the possible presence of emission arising from a ligand-centered (LC) transition, the free ligand 2-aminopyrazine was also investigated at 300 K.[12, 21] The results show two very weak emission bands at 475 and 499 nm for **1m** and **1n**, respectively, corresponding to ligand-centered $\pi \rightarrow \pi^*$ transitions (section S3, Figure S14). Moreover the influence of pyrazine substituent in the optical properties of the layers has also been evaluated by a comparative study. Although there are not enough data to get decisive conclusions, we have observed that the emission is affected by the nature of the substituent on the pyrazine ring (for additional data see SI section S3, Table S5).

The polymeric stair-type chain structure adopted by **1m** and **1n** is common for I-Cu-N donor ligands coordination polymers and the emission origin, centered around 550-630 nm, might be derived from an excited state ^{3}ILCT* in mixed character with copper cluster-centered $3d^{10} \rightarrow 3d^9 4s^1$ (^{3}MCC). The contribution of ^{3}MCC transition in the excited state is supported by the short Cu-Cu distances observed, since the half of the Cu-Cu distances are below the sum of Van der Waals radii (2.80 Å) and the broad and unstructured band observed is also in accordance with the assignation made as a combination of ^{3}(M + I)LCT states (Figure 5a).[22] Additionally, thermochromic effects can be largely affected by a change in Cu-Cu distances due to the ^{3}MCC excitation state.[23]

Therefore, in order to rationalize the origin of the enhancement in the emission when lowering the temperature, the crystal structure for **1m** was measured at 100 K (Tables S1 and S2). Thus, it can be observed that the general features of the structure of **1m** do not change with the temperature (Table S2). However, a significant shortening in the Cu-Cu distances takes place when lowering the temperature going from 2.715 Å at 296 K to 2.660 Å at 100 K (Δ= 0.055 Å) (Table S2). This shortening could be associated with an increase in the medium rigidity; when the temperature decreases. As the rest of the distances and angles do not suffer almost variation (Table S2), there is no great distortion in the sheets, allowing an increase in the metal-metal bonding, and thus the energy levels are lowered, shifting to blue region. The increase observed in the emission intensity upon cooling is also in according with the increase in structural rigidity, decreasing the non-radiative rate constant.[24]

In order to rationalize the thermochromic effect evidenced by the experiments we have performed calculations of the excitation spectra for the two structures of the $[Cu_2I_2(Apyz)]_n$ compound resolved by X-ray diffraction at low (100 K) and high (296 K) temperatures (Figure 5b). Our theoretical approach is able to capture the reduction in the photoluminescence performance observed from the low-temperature to the high-temperature regimes. In this case, the Figure 5b shows the prominent excitation feature located at 526 nm for the case of T= 100 K. Nevertheless, the intensity of the peak decreases around a 30 % for the case of T= 296 K w.r.t. the T=100 K case, with the maximum of the peak located at 530 nm.

Unfortunately, as expected, theory is not able to reproduce the total vanishing of the photoluminescent response at 300 K observed in the experiment, and the 30% reduction in the theoretical intensity of Figure 5b is just a reflection of the slight geometrical changes between the two structures. Specifically, the total vanishing of the photoluminescence response may have its origin in the thermal fluctuations (not accounted by theory) that tend to broaden both valence and conduction bands, subsequently reducing the efficiency of the metal-to-ligand transition for the case of the high-temperature regime as compared with the T=100 K case. Nevertheless, the theoretical prediction shows an excellent agreement with the experimental observation of the photoluminescence reduction (Figure 5a).

2.2.1.1 On-surface thermochromic properties of 1n nanolayers: The thermochromic properties of isolated **1n** nanolayers deposited on SiO_2 have also been studied. Figure 6a shows topological AFM images with their corresponding height profiles showing three different **1n** nanolayers with over micron size lateral dimensions, and *ca.* 100, 200 and 350 nm thicknesses. Figure 6b displays an optical image of the AFM analyzed area. Figures 6c-e show confocal microscopy images of the same region upon irradiation with a laser with excitation wavelengths of 351 and 364 nm at a power of 9.36 µW at 300 K, A-C nanolayers show bright emission between 500 and 600 nm (Figure 6c). However, the emission of the A-C nanolayers is significantly reduced (not perceptive under confocal microscope) when laser power is reduced to 6.34 µW (Figure 6d), and it becomes more intense at 80 K (Figure 6e). The emission observed at 80 K reverses to the initial state as the sample reaches the initial temperature. Therefore, the thermochromism observed in these nanolayers is reversible.

2.2.2 Mechanochromic bevahior—Pressed pellets of **1n** and **1m** were prepared at different pressures ranging from 1 to 5 GPa. Interestingly, no emission is observed in **1n** and **1m** pellets even when the temperature decreases to 80 K (Figure 7). However, when a pellet is ground it apparently recovers its previous behavior. Despite these changes, the X-ray powder diffraction patterns of the ground and unground pellets do not differ significantly from those of the solid and crystals (Sect. S3, Figure S15).

In order to understand the decrease in the emission intensity as a consequence of the pressure, we subjected a crystal of **1m** to a high-pressure study, analyzing the variation in its structure and emission, and performed theoretical calculations using density functional theory (DFT).

A single crystal of compound **1m** has been subjected to an emission study *versus* pressure (Figure 8b). The low pressure (≈ 0 GPa) spectrum consists of a non-symmetric broadband peaking around 645 nm. Upon applying pressure two different behaviors can be observed, on the one hand there is a pronounced linear red-shift of the maximum of the band of around 15 nm/GPa reaching at approximately 690 nm and simultaneously a gradual quenching of its intensity up to 5 GPa appeared, vanishing beyond that pressure. At around 4 GPa two emission bands are present with maxima at 560 nm and around 690 nm, the latter band cannot be fully characterized due to the overlapping with the ruby emission (Figure 8b and Figure S16). The emergence of another broadband blue-shifted respect to the previous one remains up to 8.7 GPa with no significant changes in its maxima at around 590 nm. Upon gradual release of pressure the spectra tend to recover their previous emission shapes (Figure S16).

As we have mentioned above, it is quite common in the CuI-L complexes to relate the low energy emission band to a triplet metal cluster centered excited state (^{3}MCC*) involving a CuI core, mixture of ^{3}IMCT (charge transfer from iodine 5p to copper 4s) and a metal cluster centered [^{3}MCC*, $d_{Cu}\rightarrow(s, p)_{Cu}$] in orbital parentage.[25] These transitions are difficult to distinguish experimentally and pressure can be a method to separate both contributions.

As commented above, in our case there are two different pressure behaviors of the emission band. At ambient conditions the Cu1-Cu1a distance is lower than the Van der Waals limit (2.8 Å), which leads to think in cuprophilic interactions as the main responsible for the emission observed, although other contributions (^{3}IMCT) can also be considered. The fact that upon applying pressure the Cu-I distances shorten around a 2 %, less than the double for the Cu-Cu (~ 4.4 %) distance in the pressure range from 0 to 4.5 GPa, induces to think that changes in the emission spectra (Figure 8b) can be correlated with the shortening of the Cu-Cu distance, and the red shift of the band can be explained on the basis that Cu-Cu interactions in the lowest unoccupied molecular orbital (LUMO) have bonding character and the shortening of these distances increases the bonding character and consequently the energy level is lowered giving rise to a red shift of the band. However, the intensity of this emission gradually decreases until its complete disappearance at P > 5 GPa and other unstructured band appears around 590 nm. The fact that no pressure shifting of the latter emission peak is observed, together with the negligible pressure changes in the Cu1-I1 and Cu1-I1a distances (~1 %) in the 5-8.5 GPa pressure range, may suggest a ^{3}IMCT origin for this band.

To ensure these observations, the computed GW-BSE photoexcitation spectra for compound $[Cu_2I_2(Apyz)]_n$ at different externally applied hydrostatic pressures (Figure 8a), have been obtained, exhibiting a prominent excitation feature associated to MLCT metal-to-ligand transitions, produced typically between VB-1/VB and CB/CB+1,[26] which mostly locate in the metal skeleton and in the organic ligands, respectively. Interestingly, as the pressure starts to increase this excitation feature goes progressively decays, in excellent agreement with the experimental photoluminescence spectra (Figure 8b), where the photoluminescence substantially vanishes for high pressures. For increasing values of the pressure, theory predicts a slight shift of the peak up to slightly higher wavelengths from 535 nm for the case

of P = 0 to 538, 542, 546, 551 nm for 2.53, 4.75, 6.44 and 8.35 GPa, respectively, in agreement with the experimental data. Nevertheless, this shift should be taken cautiously since these small variations could be framed within the accuracy of this approach.

X-ray diffraction studies on a single crystal of **1m** were carried out to analyze structural changes with the pressure. Thus, a crystal of **1m** has been introduced into a cell together with a liquid medium and has undergone a gradual increase of the pressure from 0 to 8.35 GPa. The data obtained from this experiment allow calculating the isothermal equations of state (*EoS*) and the bulk modulus (K_o = 14,1(3)) (see section S1, Figures S4-S8 and Table S3), explaining the degree of material compressibility, which is in the range of the organometallic compounds. Additionally the increase of pressure induces a significant variation in some distances and angles of the structure (Table 1 and Figure S9). Thus, among the general shortening of distances the most significant variation is found in Cu-Cu distances decreasing to 17.21 % (Cu-Cu^{iii}) when pressure increases to 8.35 GPa (Table 1). Other significant distortions with the pressure are reflected in the corresponding Cu–I–Cu and I–Cu–I bond angles along the chain (75.07 º for 0 GPa to 63.85 º at 8.35 GPa and 104.93 º for 0 GPa to 116.15 at 8.35 GPa, respectively) (Figure S9). Finally, the interlayer distances decrease from 4.22 Å, at atmospheric pressure, to 3.31 Å at 8.35 GPa.

Theoretical calculations have been carried out in order to understand these observations. Thus, the vanishing of this excitation feature as the pressure increases may be explained in terms of the pressure-induced electronic degeneracy rupture (explained in detail on the basis of the computed quasi-particle GW-corrected density of states, section S4, Figure S17). First, the mentioned emerging degeneracy-rupture produces a loss of efficiency in the metal-ligand transition; responsible for the photoluminescent behavior since highly degenerated electronic orbitals contributing to that transition slightly modify their occupancy and symmetry by effect of pressure (Figure 9 and Figure S17). Furthermore, and intimately linked to the latest comment, with the increasing pressure certain bond lengths within the compound non-negligibly compress, which is the case of the Cu-Cu bond (around a 20% of bond-length compression followed by a reduction of around 3° in the I-Cu-I-Cu dihedral angle from 0 to 9 GPa). In particular, this reduction in the Cu-Cu bond, which accommodates occupied electronic states that actively participate in the permitted metal-to-ligand transition (cuprophilic interaction), has its reflection in a visible vanishing of the photoluminescence. As aforementioned, in the case of the Cu-Cu bonding, electrons belonging to the slightly hybridized occupied Cu dz^2 orbitals (within the Cu-Cu bond) are pushed towards each other by the effect of the pressure forcing them to occupy the same electronic state. Nevertheless, the system reacts by the electronic degeneracy rupture, slightly modifying the orbital orientation. For the case of P = 0 the slightly hybridized dz^2 orbitals located in each Cu atom are oriented facing their respective lobes to maximize the cuprophilic interaction, and thus, the photoluminescence becomes significant (Figure 9). Nevertheless, for high pressures, with a reduced Cu-Cu bond length, the lobes of the dz^2 orbitals spin in such a way to avoid the electronic overlapping. This behavior produces a reduction in the metal-to-ligand transition efficiency, which finally leads to the photoluminescence vanishing.

2.2.3 Electrical properties and sensing behavior—The interesting electrical properties already reported for materials based on Cu_2I_2 chains prompted us to characterize **1m**.[18, 27] Thus, single crystals of **1m** display a DC electrical conductivity of 8.6×10^{-7} Scm^{-1} at room temperature and a classical semiconducting behavior, with activation energy of 65 meV (Figures S19 and S20). The temperature dependence study does not show any phase transition in the range 100-400 K (Figure S19).

We previously reported that materials based on Cu_2I_2 chains bearing terminal ligands with H-bonding capabilities undergo a significant change in their conductivity upon exposition to specific organic solvents.[27] Therefore, we have extended our study using AC conductivity measurements. Thus, the initial conductivity of *ca.* 1.32×10^{-8} Scm^{-1} enhances to 2.83×10^{-8} Scm^{-1} and up to 3.61×10^{-7} Scm^{-1} after 4 and 24 h, respectively, upon exposition of the **1m** pellets to acetic acid vapors (Figure S21). This chemical response can be ascribed to hydrogen-bond interactions between the acetic acid and the amino group of the 2-aminopirazine ligand similarly to that observed in the related $[CuI(ANP)]_n$ (ANP= 2-amino-5-nitropiridiyne).[18, 27]

2.2.4 Electrochemical studies—The electrochemical behavior of the $[Cu_2I_2(Apyz)]_n$ modified carbon paste electrode in 0.5M K_2SO_4 under different scan rates was investigated, in the potential range -0.5 and 0.65V vs Ag/AgCl/KCl sat (see section S7). A pair of quasi-reversible redox peaks (IpA and IpC) have been observed (Figure S24). These peaks should be ascribed to the redox pair Cu^{II}/Cu^{I}. The mean peak potential is $E_{1/2}$ = (Epc+Epa)/2 = 163 mV (scan rate 500 $mV.s^{-1}$). With the scan rate, both the anodic and the cathodic peak potentials shift towards the positive and negative direction respectively. The anodic and the cathodic peak currents are proportional to the scan rate up to 500 $mV.s^{-1}$. This behavior could be related with a surface controlled redox process.[28]

3 Conclusions

Micro and nanolayers of Cu_2I_2 chains connected by 2-aminopyrazine have been prepared by direct synthesis. The high stimuli-response sensibility already found in Cu_2I_2 chains bearing terminal ligands with H-bonding capabilities has been extended to its related bidimensional structure $[Cu_2I_2(Apyz)]_n$. Thus, we have found that materials at the micro and nanoscale of $[Cu_2I_2(Apyz)]_n$ are multifunctional, showing semiconductivity and luminescence. Additionally these materials present reversible response to both temperature and pressure. Thus, when lowering the temperature a dramatic increase in its emission is observed, and while increasing the pressure its emission decreases. Additionally, as in its related monodimensional Cu_2I_2 chains, the presence of acetic acid vapors enhances its electrical conductivity.

Interestingly, these reversible physical responses can be rationalized analyzing the structural changes of $[Cu_2I_2(Apyz)]_n$ with the temperature and pressure. Thus, the strong emission at low temperature is caused by the temperature-dependence in Cu-Cu distances, which decreases when lowering the temperature, being the key parameter that influences the luminescence properties of the ^{3}MCC transition. However, the mechanochromic studies show a more complex structural distortion with a shortening in the Cu-Cu distances and in

the dihedral, Cu-I-Cu and I-Cu-I angles. Interestingly, the DFT studies show that although pressure produces a shortening in the Cu-Cu distances it also generates electronic degeneracy-rupture which modifieds the orbital orientation avoiding the orbital overlapping and reducing the metal-to-ligand transition efficiency, which finally leads to the photoluminescence vanishing.

To sum up, we can conclude that materials based on Cu_2I_2 chains bearing different terminal or bridging ligands with H-bonding capabilities show interesting electronic properties, e.g. luminescence and/or electrical conductivity, and they are an excellent novel source of valuable stimuli-response materials. This is due to high structural flexibility of the Cu_2I_2 chains and how small structural variations drastically modify their physical properties. Finally, it is worth mentioning that the simple preparation procedures of these materials as well as the industrial availability of their building blocks, e.g. 2-aminopyrazine and CuI, together with their physico-chemical properties, suggest their high potential towards applications, such as sensors/nanosensors.

4 Experimental Section

All reagents and solvents purchased were used without further purification.

IR spectra were recorded with a PerkinElmer 100 spectrophotometer using a universal ATR sampling accessory from 4000–650 cm^{-1}. Elemental analyses were performed with a LECO CHNS-932 Elemental Analyzer. Powder X-ray diffraction data was collected using a Diffractometer PANalytical X'Pert PRO θ/2θ primary monochromator and detector with fast X'Celerator. The samples have been analyzed with scanning θ/2θ. Scanning Electron Microscopy (SEM) images were taken in a Philips XL 30 S-FEG electron microscope, applying an electron beam of 300 μA intensity and 10 kV potential, at a pressure of 10^{-7} Pa. Atomic Force Microscopy images were registered in a Nanotec Electronica microscope, at room temperature and in an open atmosphere, using Olympus cantilevers with a constant nominal force of 0.75 N/m. Images were processed by the use of the WSxM program.[21c]

Luminescence excitation and emission spectra of the microcrystals and nanosheets of $[Cu_2I_2(Apyz)]_n$, were performed with a Jobin-Yvon Horiba Fluorolog FL-3-11 spectrometer fitted with a JY TBX picosecond detection module using band pathways between 1-2 nm for both excitation and emission. Measurements at variable temperature were done using an Oxford Cryostat Optistat DN with an accessory for solid samples. Lifetimes measurements were recorded with a Fluoromax phosphorimeter accessory containing a UV xenon flash tube. Lifetime data were fitted by using the Jobin-Yvon software package and the Origin Pro 8 program.

Luminescence images and emission spectra of nanostructures deposited on SiO_2 surfaces were performed in a Leica TCS SP2 spectral confocal microscope with three adjustable internal detection channels for band width and wavelength and a transmitted illumination external detector for clear field images. The excitation of the samples was done with laser lines with wavelengths of 351 and 364 nm simultaneously.

X-ray diffraction data collections and the structure determination at 100 K were done with a Bruker Kappa Apex II diffractometer with graphite-monochromated $Mo_{K\alpha}$ radiation (λ=0.71073 Å). The cell parameters were determined and refined by a least-squares fit of all reflections. A semi-empirical absorption correction (SADABS) was applied. All the structures were solved by direct methods using the SIR92 program[29] and refined by full-matrix least-squares on F^2 including all reflections (SHELXL97).[30] All non-hydrogen atoms were refined anisotropically. The hydrogen atoms were included in their calculated positions and refined riding on the respective parent atoms. All calculations were performed using the WINGX crystallographic software package.[31]

The rest of single crystal X-ray diffraction (HP-SCXRD) measurements were made at room temperature using a Rigaku SuperNOVA diffractometer equipped with an EOS detector (CCD) and Mo radiation micro-source. All measurements were processed with the CrysAlisPro software.[32] The structure of the compound was determined by a dual-space algorithm using the SHELXT program,[33] and refinement was performed using SHELXL program[34] against F^2 by full-matrix least-squares refinement. All non-hydrogen atoms were refined anisotropically and hydrogen atoms were included in the model at calculated positions, and refined with a rigid model with their U_{iso} value to $1.2U_{eq}$ of their parent atoms. The PLATON program[35] has been used for geometric calculations.

[CCDC 1538152-1538167 contains the supplementary crystallographic data for this paper. These data can be obtained free of charge from The Cambridge Crystallographic Data Centre via www.ccdc.cam.ac.uk/data_request/cif.].

For high-pressure measurements, we have used a Diacell Bragg-S diamond anvil cell (DAC) from Almax-EasyLab, with an opening angle of 90º and anvil culets of 600 µm diameter, fitted with a stainless gasket containing a hole of 200 µm diameter and 60 µm depth.

The high-pressure luminescence spectra were recorded on a 0.75 m single grating monochromator (Spex 750M). The excitation source is a 375 nm diode laser excitation (BrixX 200mW pump power) and a cooled photomultiplier (PMT) (Hamamatsu 928b) were used in detection.

Theoretical studies were carried out using a wide battery of first-principles DFT-based calculations to compute mechanical and electronic properties, total energies and many-body excitation spectra.

*Synthesis of $[Cu_2I_2(Apyz)]_n$ in a micrometric size (***1m***).* A mixture of copper(I) iodide (50 mg, 0.26 mmol) and 2-aminopyrazine (Apyz) (12 mg, 0.13 mmol) was dissolved in 15 mL of acetonitrile-water (1:1). The yellow solution was sealed in a 23 mL Teflon-lined stainless steel autoclave, heated at 140 ºC for 48 h and cooled to 20 ºC at 5.0 ºC/min. The resulting mixture consisted of a colorless solution and yellow crystals. Single crystals suitable for X-ray diffraction were filtered off, washed with acetonitrile (2 x 5 mL), ethanol (2 x 3 mL) and diethyl ether (2 x 3 mL), and dried in vacuum. Yield: 38 mg (62 % based on Cu). Anal. Calcd (%) for $C_4H_5Cu_2I_2N_3$: C 10.09, H 1.06, N 8.83; found: C 10.38, H 1.08, N 8.91; IR selected data (ATR): ν (cm^{-1}) = 3419 (s), 3316 (s), 3190 (w), 3024 (w), 1901 (w), 1613 (vs), 1604 (vs), 1583 (vs), 1523 (vs), 1470 (s), 1435 (vs), 1351 (s), 1316 (s), 1206 (vs), 1168

(m), 1068 (s), 1046 (m), 1026 (vs), 897 (m), 868 (w), 818 (vs), 743 (m). XRD powder diffraction confirmed the purity of the sample.

*Synthesis of $[Cu_2I_2(Apyz)]_n$ in a nanometric size (***1n***).* Copper(I) iodide (51 mg, 0.27 mmol) was dissolved in 10 mL of acetonitrile; on the other hand, 2-aminopyrazine (Apyz) (13 mg, 0.14 mmol) was dissolved in 3 mL of distilled water. Both solutions were mixed and magnetically stirred at 25 ºC for 5 minutes, at a speed of 500 rpm. The resulting mixture consisted of a yellowish solution and a yellow solid formed of layers. The solid was filtered off, washed with acetonitrile (2 x 5 mL), water (2 x 5 mL) and ethanol (2 x 3 mL), and dried in vacuum. Yield: 43 mg (67 % based on Cu). Anal. Calcd (%) for $C_4H_5Cu_2I_2N_3$: C 10.09, H 1.06, N 8.83; found: C 10.53, H 1.18, N 8.82; IR selected data (ATR): ν (cm^{-1}) = 3426 (s), 3321 (s), 3190 (w), 3024 (w), 1901 (w), 1615 (vs), 1606 (vs), 1584 (vs), 1524 (vs), 1471 (s), 1437 (vs), 1351 (s), 1317 (s), 1208 (vs), 1169 (m), 1069 (s), 1049 (m), 1027 (vs), 898 (m), 820 (vs), 744 (m). XRD powder diffraction confirmed the purity of the sample.

Supporting Information

Refer to Web version on PubMed Central for supplementary material.

Acknowledgements

We thank financial support from the Spanish Ministerio de Economía y Competitividad (MAT2013-46502-C2-2P, MAT2016-77608-C3-1-P, MAT2016-75883-C2-2-P, MAT2010-20843-C02-01, MAT2016-75586-C4-4-P, CTQ2016-75816-C2-1P). Also to the scientific computing center (CCC) of the Autonoma University of Madrid for their time. JIM acknowledges the financial support by the “Ramón y Cajal” Program of MINECO (Grant RYC-2015-17730) and the EU via the ERC-Synergy Program (Grant ERC-2013-SYG-610256 NANOCOSMOS).

References

[1]. a) Cui Y, Yue Y, Qian G, Chen B. Chem Rev. 2012; 112:1126–1162. [PubMed: 21688849] b) Hashemi M, Mohandes F, Salavati-Niasari M, Esmaeily AS. J Mater Sci-Mater El. 2015; 26:6860–6867.c) Errandonea D, Muñoz A, Gonzalez-Platas J. J Appl Phys. 2014; 115:216101.

[2]. Kurmoo M. Chem Soc Rev. 2009; 38:1353–1379. [PubMed: 19384442]

[3]. Givaja G, Amo-Ochoa P, Gomez-Garcia CJ, Zamora F. Chem Soc Rev. 2012; 41:115–147. [PubMed: 21713280]

[4]. Hu L, Lyu SY, Fu F, Huang JD, Wang SQ. J Mater Sci. 2016; 51:2716–2726.

[5]. a) Chowdhury MA, Joshi M, Butola BS. J Eng Fibers and Fabrics. 2014; 9:107–123.b) Lopez IS, Mendonca AL, Fernandes M, Bermudez VD, Morgado J, Del Pozo G, Romero B, Cabanillas-Gonzalez J. Opt Mater. 2012; 34:1447–1450.

[6]. Gao YZ, Yao WH, Sun J, Zhang HM, Wang ZD, Wang L, Yang DK, Zhang LY, Yang H. J Mater Chem A. 2015; 3:10738–10746.

[7]. a) Benito Q, Le Goff XF, Nocton G, Fargues A, Garcia A, Berhault A, Kahlal S, Saillard JY, Martineau C, Trebosc J, Gacoin T, et al. Inorg Chem. 2015; 54:4483–4494. [PubMed: 25857746] b) Krishnakumar R, Kraus WL. Mol Cell. 2010; 39

[8]. Savchuk OA, Carvajal JJ, Cascales C, Massons J, Aguilo M, Diaz F. J Mater Chem C. 2016; 4:6602–6613.

[9]. Amo-Ochoa P, Welte L, Gonzalez-Prieto R, Sanz Miguel PJ, Gomez-Garcia CJ, Mateo-Marti E, Delgado S, Gomez-Herrero J, Zamora F. Chem Commun. 2010; 46:3262–3264.

[10]. Zhou H-C, Long JR, Yaghi OM. Chem Rev. 2012; 112:673–674. [PubMed: 22280456]

[11]. a) Vegas VG, Lorca R, Latorre A, Hassanein K, Gómez-García CJ, Castillo O, Somoza Á, Zamora F, Amo-Ochoa P. Angew Chem Int Ed. 2017; 56:987–991.b) Rodriguez-San-Miguel D,

Amo-Ochoa P, Zamora F. Chem Commun. 2016; 52:4113–4127.c) Rodenas T, Luz I, Prieto G, Seoane B, Miro H, Corma A, Kapteijn F, Llabrés i Xamena FX, Gascon J. Nat Mater. 2015; 14:48–55. [PubMed: 25362353] d) Neaime C, Daiguebonne C, Calvez G, Freslon S, Bernot K, Grasset F, Cordier S, Guillou O. Chem Eur J. 2015; 21:17466–17473. [PubMed: 26471940] e) Sakamoto R, Hoshiko K, Liu Q, Yagi T, Nagayama T, Kusaka S, Tsuchiya M, Kitagawa Y, Wong W-Y, Nishihara H. Nat Commun. 2015; 6:6713. [PubMed: 25831973] f) Sakamoto R, Yagi T, Hoshiko K, Kusaka S, Matsuoka R, Maeda H, Liu Z, Liu Q, Wong W-Y, Nishihara H. Angew Chem Int Ed. 2017; 56:3526–3530.

[12]. Manbeck GF, Brennessel WW, Evans CM, Eisenberg R. Inorg Chem. 2010; 49:2834–2843. [PubMed: 20158202]

[13]. a) Hassanein K, Amo-Ochoa P, Gomez-Garcia CJ, Delgado S, Castillo O, Ocon P, Martinez JI, Perles J, Zamora F. Inorg Chem. 2015; 54:10738–10747. [PubMed: 26501154] b) Cariati E, Bourassa J. Chem Commun. 1998:1623–1624.

[14]. a) Goher MAS, Bitschnau B, Sodin B, Gspan C, Mautner FA. J Mol Struct. 2008; 886:32–38.b) Boonmak J, Nakano M, Chaichit N, Pakawatchai C, Youngme S. Inorg Chem. 2011; 50:7324–7333. [PubMed: 21728325] c) Shirvan MRASA, Aghajeri M, Haydari Dezfuli S, Hossini F. Acta Cryst Sect E. 2012; E68:m303.d) Pospisil J, Jess I, Nather C, Necas M, Taborsky P. New J Chem. 2011; 35:861–864.e) Kitada N, Ishida T. CrystEngComm. 2014; 16:8035–8040.

[15]. Araki H, Tsuge K, Sasaki Y, Ishizaka S, Kitamura N. Inorg Chem. 2005; 44:9667–9675. [PubMed: 16363835]

[16]. Aguirrechu-Corneron A, Hernandez-Molina R, Rodriguez-Hernandez P, Munoz A, Rodriguez-Mendoza UR, Lavin V, Angel RJ, Gonzalez-Platas J. Inorg Chem. 2016; 55:7476–7484. [PubMed: 27429246]

[17]. Hassanein K, Conesa-Egea J, Delgado S, Castillo O, Benmansour S, Martinez JI, Abellan G, Gomez-Garcia CJ, Zamora F, Amo-Ochoa P. Chem Eur J. 2015; 21:17282–17292. [PubMed: 26439771]

[18]. Amo-Ochoa P, Hassanein K, Gomez-Garcia CJ, Benmansour S, Perles J, Castillo O, Martinez JI, Ocon P, Zamora F. Chem Commun. 2015; 51:14306–14309.

[19]. Zhao J, Wang Y-N, Dong W-W, Wu Y-P, Li D-S, Zhang QC. Inorg Chem. 2016; 55:3265–3271. [PubMed: 26967044]

[20]. Wu F, Tong H, Li Z, Lei W, Liu L, Wong W-Y, Wong W-K, Zhu X. Dalton Trans. 2014; 43:12463–12466. [PubMed: 24886808]

[21]. a) Cariati E, Lucenti E, Botta C, Giovanella U, Marinotto D, Righetto S. Coord Chem Rev. 2016; 306(Part 2):566–614.b) Tsuge K, Chishina Y, Hashiguchi H, Sasaki Y, Kato M, Ishizaka S, Kitamura N. Coord Chem Rev. 2016; 306(Part 2):636–651.c) Liu W, Fang Y, Wei GZ, Teat SJ, Xiong K, Hu Z, Lustig WP, Li J. J Am Chem Soc. 2015; 137:9400–9408. [PubMed: 26151729]

[22]. Zink DM, Volz D, Baumann T, Mydlak M, Flügge H, Friedrichs J, Nieger M, Bräse S. Chem Mater. 2013; 25:4471–4486.

[23]. a) Ford PC, Cariati E, Bourassa J. Chem Rev. 1999; 99:3625–3648. [PubMed: 11849032] b) Vega A, Saillard J-Y. Inorg Chem. 2004; 43:4012–4018. [PubMed: 15206883] c) De Angelis F, Fantacci S, Sgamellotti A, Cariati E, Ugo R, Ford PC. Inorg Chem. 2006; 45:10576–10584. [PubMed: 17173412] d) Perruchas S, Tard C, Le Goff XF, Fargues A, Garcia A, Kahlal S, Saillard J-Y, Gacoin T, Boilot J-P. Inorg Chem. 2011; 50:10682–10692. [PubMed: 21957984] e) Liu Z, Djurovich PI, Whited MT, Thompson ME. Inorg Chem. 2012; 51:230–236. [PubMed: 22133068]

[24]. Berberan-Santos, BVaMN. Second Edition. Wiley-VCH Verlag GmbH & Co. KGaA; Weinheim, Germany: 2012.

[25]. a) Tran D, Bourassa JL, Ford PC. Inorg Chem. 1997; 36:439–442.b) Cariati E, Roberto D, Ugo R, Ford PC, Galli S, Sironi A. Chem Mater. 2002; 14:5116–5123.c) Tard C, Perruchas S, Maron S, Le Goff XF, Guillen F, Garcia A, Vigneron J, Etcheberry A, Gacoin T, Boilot J-P. Chem Mater. 2008; 20:7010–7016.

[26]. Troyano J, Perles J, Amo-Ochoa P, Martínez JI, Concepción Gimeno M, Fernández-Moreira V, Zamora F, Delgado S. Chem Eur J. 2016; 22:18027–18035. [PubMed: 27809369]

[27]. Amo-Ochoa P, Hassanein K, Gómez-García CJ, Benmansour S, Perles J, Castillo O, Martínez JI, Ocón P, Zamora F. Chem Commun. 2015; doi: 10.1039/C5CC04746C

[28]. Cui J-W, An W-J, Van Hecke K, Cui G-H. Dalton Trans. 2016; 45:17474–17484. [PubMed: 27739548]

[29]. Altomare A, Cascarano G, Giacovazzo C, Guagliardi A. J Appl Crystallogr. 1993; 26:343–350.

[30]. Sheldrick, GM. SHELXL-97, Program for Crystal Structure Refinement. Universität Gottingen; 1997.

[31]. Prakash MJ, Lah MS. Chem Commun. 2009:3326–3341.

[32]. Rigaku Oxford Diffraction. CrysAlisPro Software system, version 1.171.38.41. Rigaku Corporation; Oxford, UK: 2016.

[33]. Sheldrick GM. Acta Cryst. 2015; A71:3–8.

[34]. Sheldrick GM. Acta Cryst. 2008; A64:112–122.

[35]. Spek AL. Acta Cryst. 2009; D65:148–155.

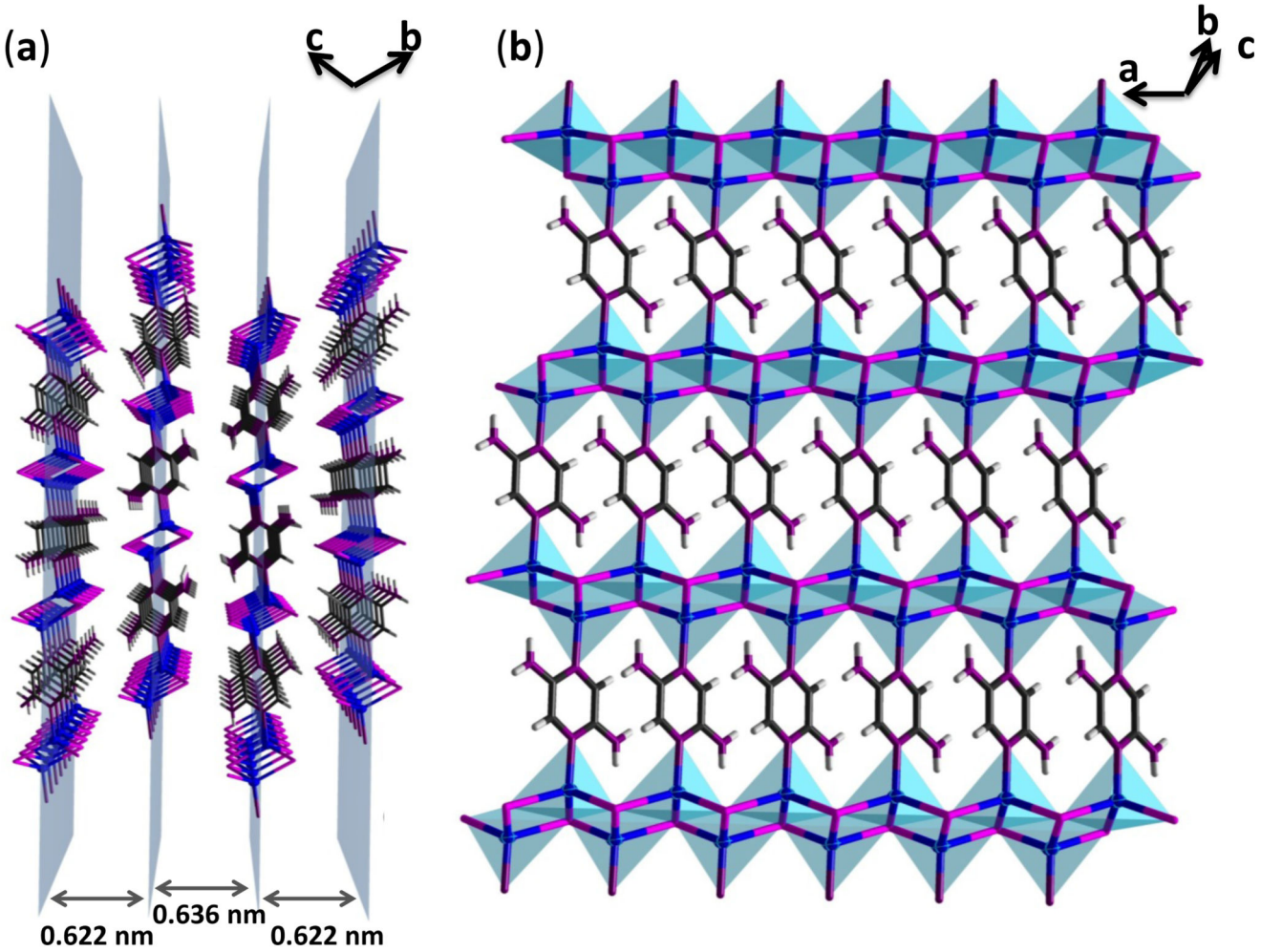

Figure 1.
Crystal structure of compound $[Cu_2I_2(Apyz)]_n$ (**1m**): lateral view with distances between layers *(a)* and frontal view of one layer *(b)*. Grey: C; white: H; violet: N; blue: Cu; pink: I.

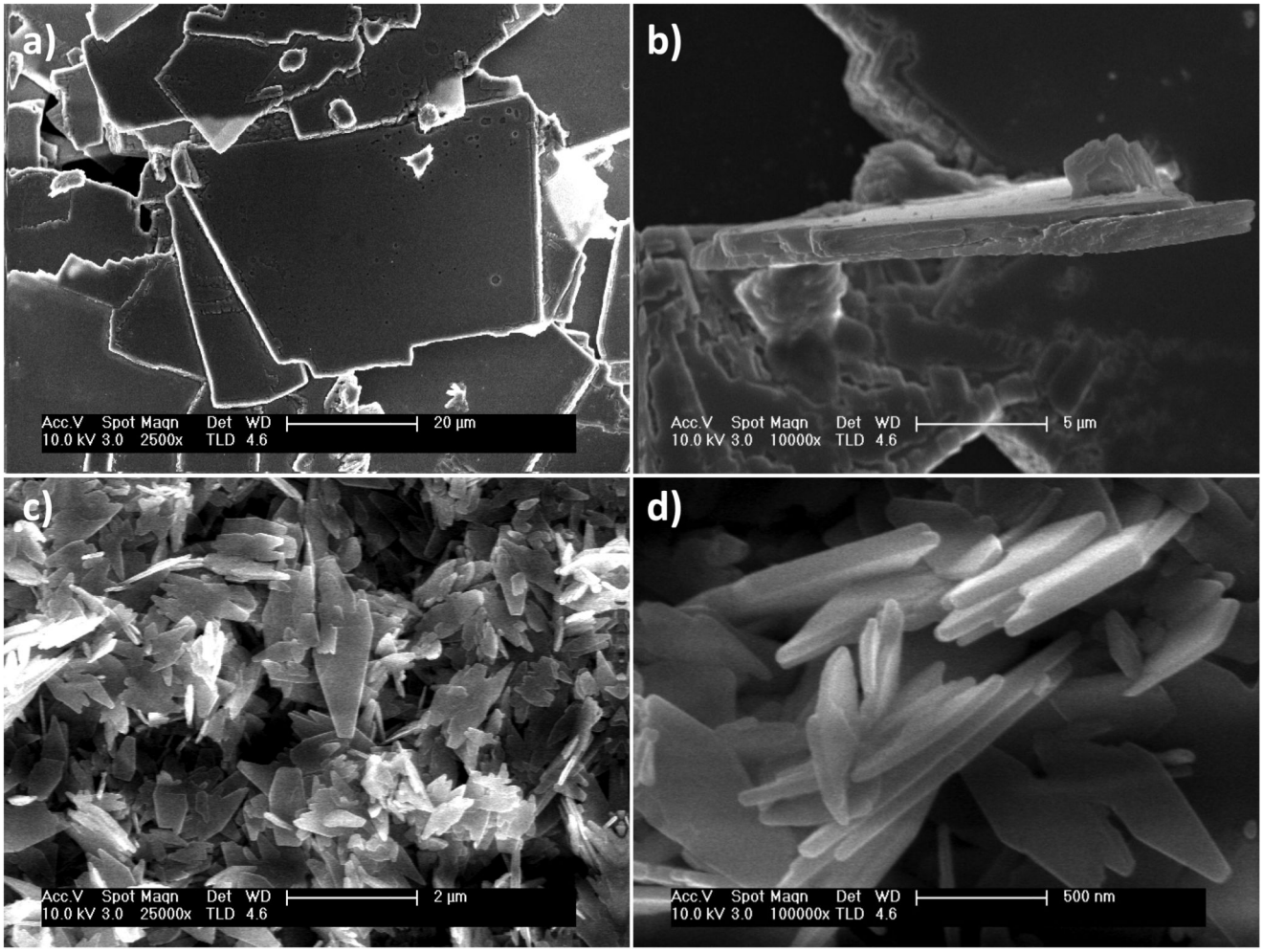

Figure 2.
(a, b) SEM images of compound **1m** microcrystals obtained by direct solvothermal reaction: large area (bar-scale 20 µm) (a) and detail of transversal image (bar-scale 5 µm) (b). (c, d) SEM images of compound **1n** layers obtained at room temperature: large area (bar-scale 2 µm) (c) and details of transversal image (bar-scale 500 nm) (d).

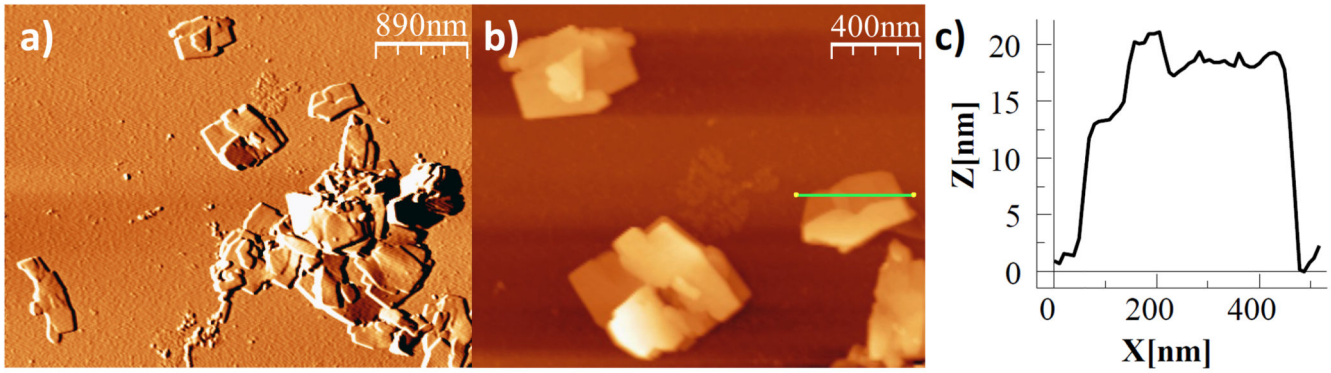

Figure 3.
(a) AFM image of compound **1n** nanosheets on SiO_2. (b) A zoomed area of a). c) A typical height profile of a nanosheet across the green line represented in b).

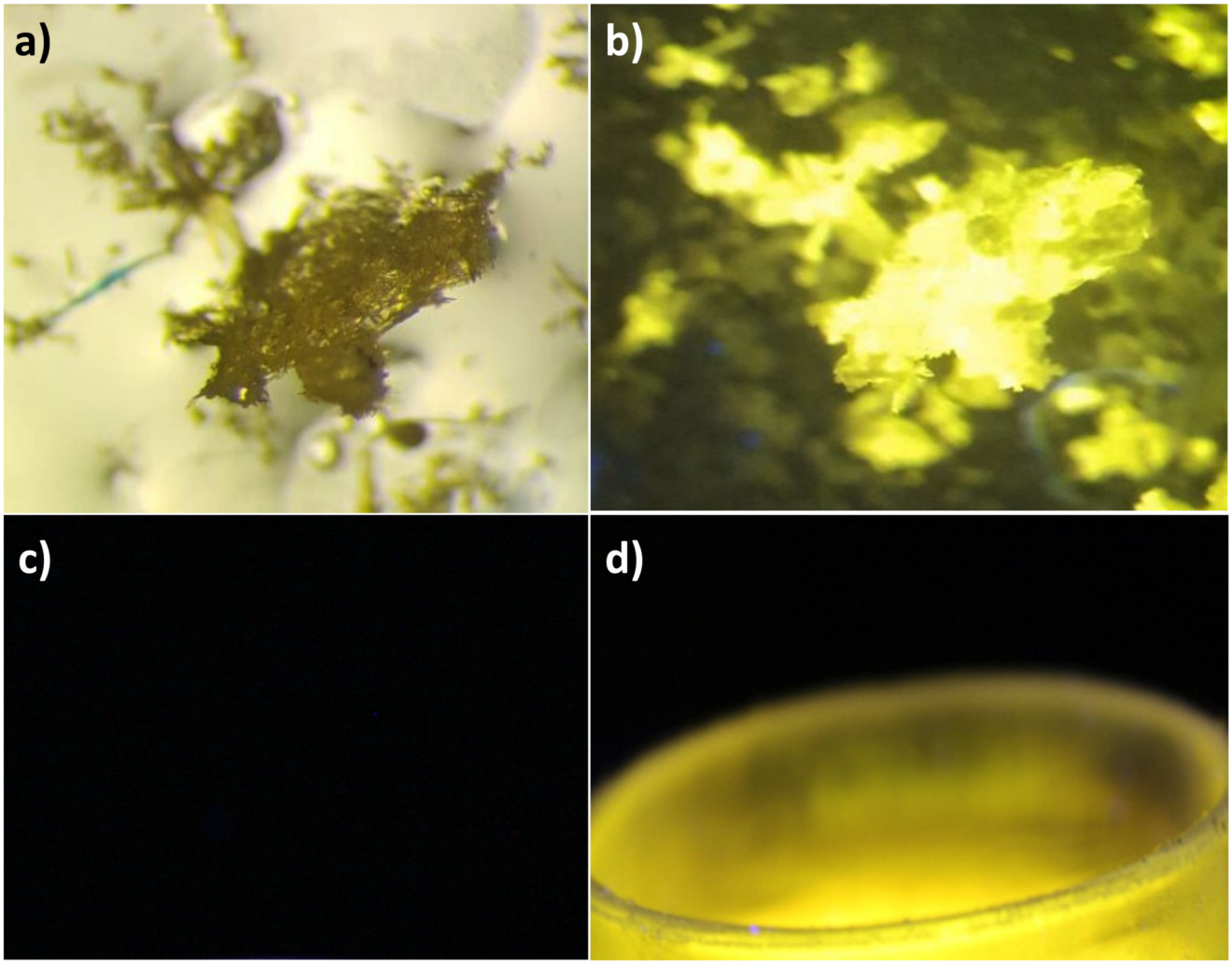

Figure 4.
(a) Optical microscope image of **1m** microcrystals at 300 K. (b) Optical microscope image of **1m** microcrystals at 80 K. (c) Photograph of **1n** crystalline powder at 300 K. (d) Photograph of **1n** crystalline powder at 80 K. All images were taken under a UV lamp with λ_{exc} = 365 nm.

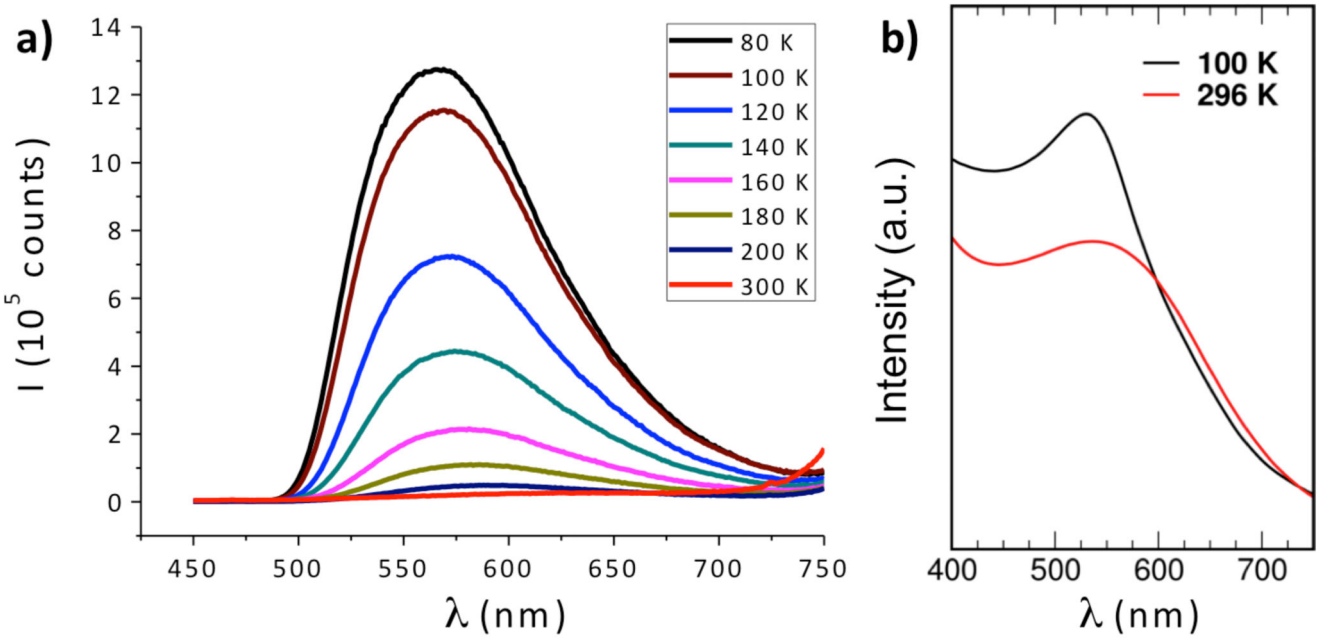

Figure 5.
(a) Emission spectra of compound **1m** at different temperatures. (b) Computed GW-BSE photoexcitation spectra of the $[Cu_2I_2(Apyz)]_n$ compound as a function of the excitation wavelength (in nm) for two structures of the $[Cu_2I_2(Apyz)]_n$ compound resolved by X-ray diffraction at low (100 K) and high (296 K) temperatures.

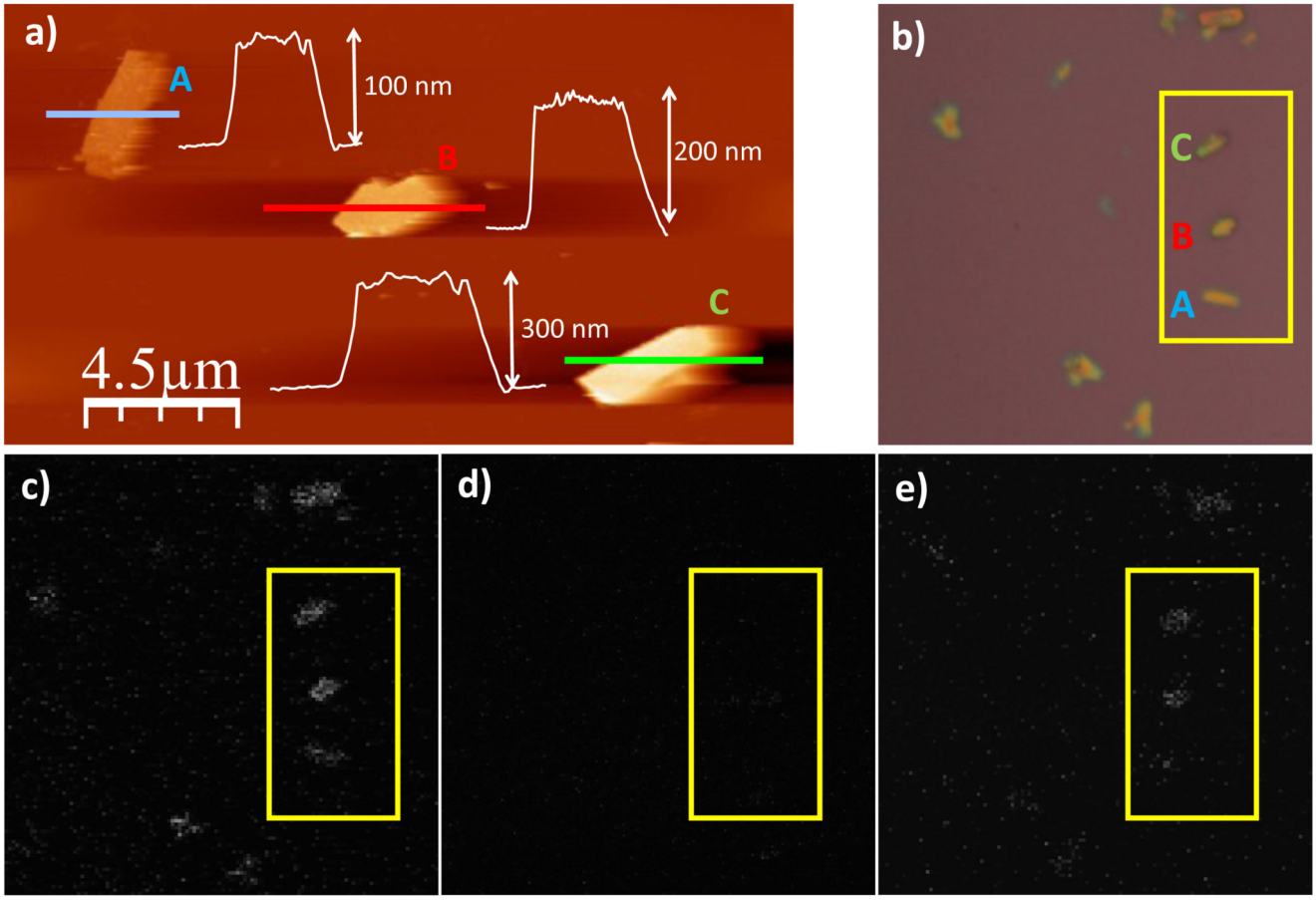

Figure 6.
a) Topographic AFM image of **1n** nanolayers deposited on a SiO_2 substrate and their height profiles, named as A-C. b) Optical microscope image of the **1n** nanolayers (A-C) characterized in a) at 298 K. c) Confocal microscopy image of **1n** nanolayers (A-C) at 300 K upon irradiation with a laser with excitation wavelengths of 351 and 364 nm, at a power of 9.36 µW. d) Confocal microscopy image of **1n** nanolayers (A-C) at 300 K, when irradiated with a laser with excitation wavelengths of 351 and 364 nm, at a power of 6.34 µW. e) Confocal microscopy image of **1n** nanolayers (A-C) 7 min. after being at 80 K, when irradiated with a laser with excitation wavelengths of 351 and 364 nm, at a power of 6.34 µW.

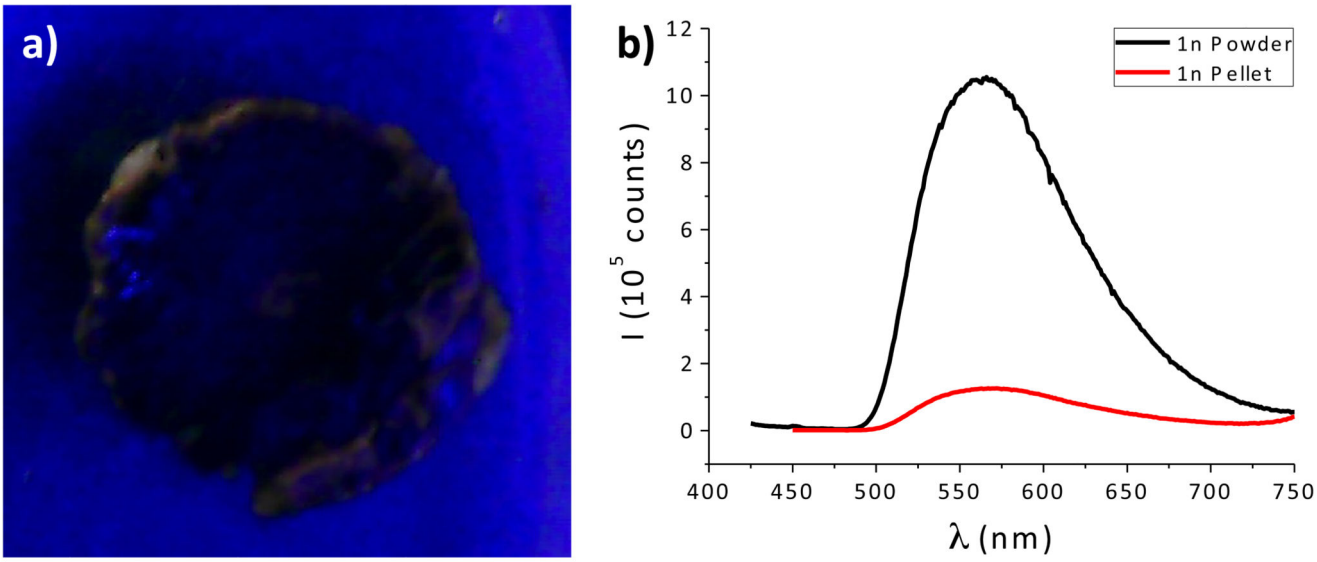

Figure 7.
(a) Detail of a single pellet prepared at a pressure of 5 GPa and its emissive behavior when exposed to liquid nitrogen; λ_{exc} = 312 nm. (b) Emission of powder (**1n**) versus pressed pellet (**1n**) at 80K.

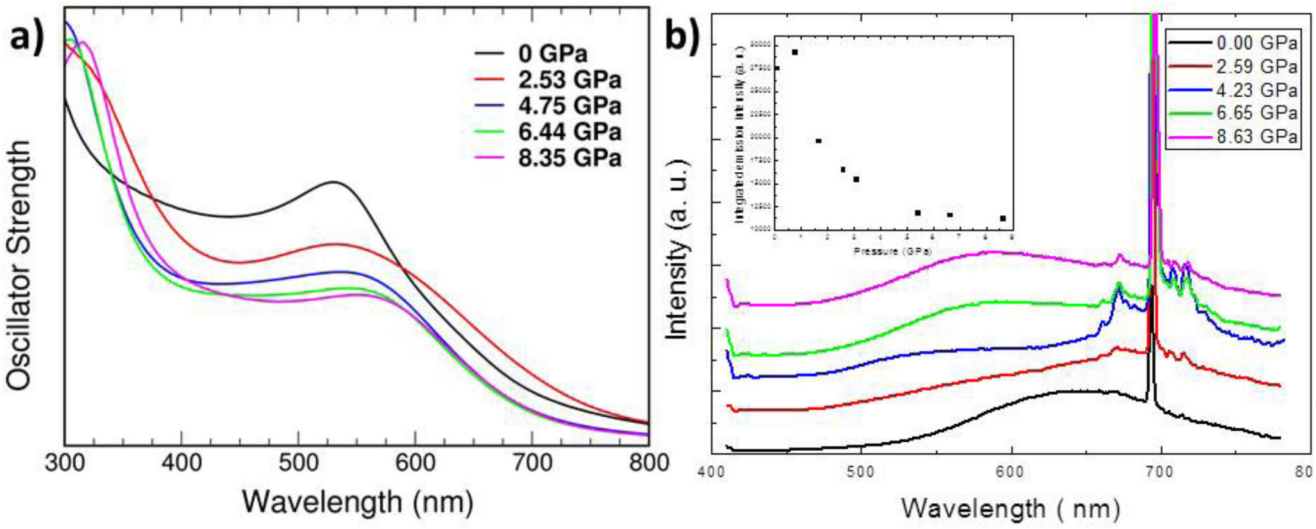

Figure 8.
(a) Computed GW-BSE photoexcitation spectra of the $[Cu_2I_2(Apyz)]_n$ compound as a function of the excitation wavelength (in nm) for different externally applied hydrostatic pressures (P=0, 2.53, 4.75, 6.44 and 8.35 GPa) within a range between 300 and 800 nm. (b) Normalized luminescence spectra of the $[Cu_2I_2(Apyz)]_n$ compound obtained at 25ºC under 375 nm laser excitation for different externally applied hydrostatic pressures (P=0, 2.59, 4.23, 6.65 and 8.63 GPa) within a range between 400 and 800 nm. The inset shows the intensity behavior with pressure. The band at 700 nm corresponds to the ruby emission.

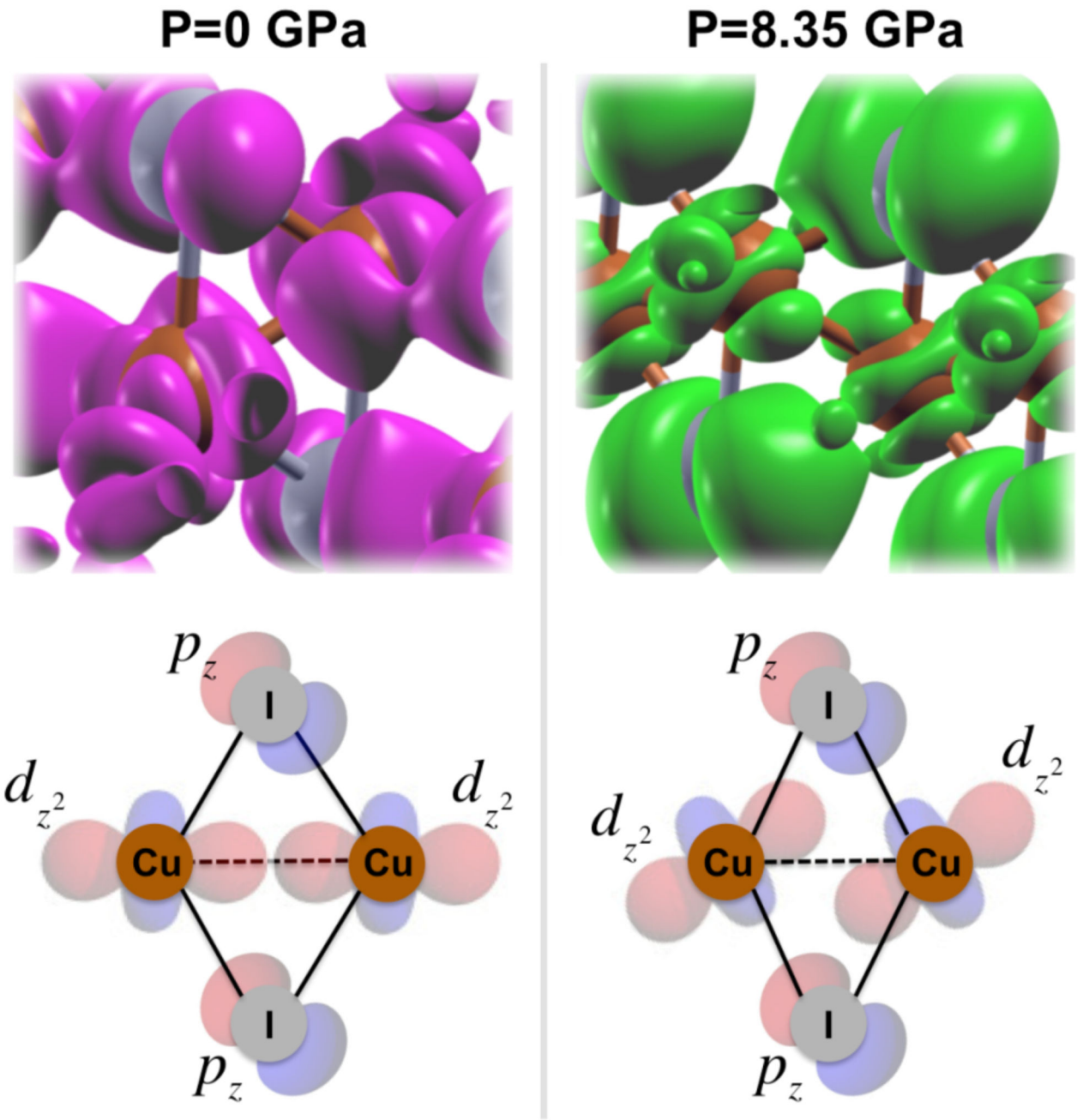

Figure 9.
(Top panels) Computed 3D valence band orbital isodensity (value of 10^{-4} $e^{-}/Å^3$) of the $[Cu_2I_2(Apyz)]_n$ compound at externally applied hydrostatic pressures of P=0 (left; purple) and 8.35 GPa (right; light green). (Bottom panels) Pictorial sketch of both situations for a better visualization.

Table 1

Most representative variation in the Cu-Cu distances and I-Cu-I and Cu-I-Cu angles for compound **1m**, from 0 GPa to 8.35GPa.

	298 K, 0 GPa	**298 K, 8.35 GPa**	**Δ**
Cu-Cu ^{ii}	2.715	2.543	-0.172 (6.34 %)
Cu-Cu ^{iii}	3.253	2.693	-0.560 (17.21 %)
I1-Cu1-I1^{i}	104.74	101.83	-2.91 (2.78 %)
I1-Cu1-I1^{ii}	118.47	121.01	+2.54 (2.14 %)
I1^{i}-Cu1-I1^{i}	104.93	116.15	+11.22 (10.69 %)
Cu1-I1-Cu1^{ii}	61.53	58.99	-2.54 (4.13 %)
Cu1^{ii}-I1-Cu1^{ii}	75.07	63.85	-11.22 (14.95 %)